A New Dynamic-Bias Measurement Setup for Nonlinear Transistor Model Identification

Valeria Vadalà, *Member, IEEE*, Antonio Raffo, *Member, IEEE*, Gustavo Avolio, *Member, IEEE*, Mauro Marchetti, Dominique M.M.-P Schreurs, *Fellow, IEEE*, and Giorgio Vannini, *Member, IEEE*

***Abstract*— In this manuscript, we present a new dynamic-bias measurement set-up and its application to the extraction of a nonlinear model for microwave field-effect transistors. The dynamic-bias technique has been recently proposed and relies on the use of low- and high-frequency vector-calibrated measurements acquired, for instance, by means of a large-signal network analyzer (LSNA). In this work, we propose a new and alternative technique to perform the dynamic-bias measurements, based on relatively low-cost instrumentation commonly available in microwave laboratories. The new acquisition system is composed by a 4-channel vector LF receiver (e.g., an oscilloscope) and a 1-channel HF scalar receiver (e.g., a spectrum analyzer), which replace the 8-channel vector receiver. Moreover, the proposed architecture greatly simplifies the measurement setup and the calibration procedure. As case study, a 0.25-μm GaN HEMT is considered. Dynamic-bias measurements, carried out by means of the proposed measurement setup, are used for the identification of a nonlinear model of this device. Finally, the model is fully validated through comparison with time-domain harmonic load-pull measurements carried out at 5 GHz.**

***Index Terms*—Dynamic-bias, FETs, harmonic load-pull measurement, nonlinear measurements, nonlinear models, semiconductor device measurements**

I. Introduction

MODELING of transistors is a very important topic in the context of microwave and millimeter wave circuit design. Well-assessed technologies as well as state-of-the-art devices need to be accurately modeled if one wants to minimize errors in the design phase when using the models in a CAD simulation environment. Although most foundries make their own models available, often a custom model tailored to the specific application considered (e.g., high-efficiency power amplifiers, mixers, etc.) must be extracted.

A custom model is needed, for example, when dealing with GaN devices to accurately account for low-frequency (LF) dispersion phenomena that strongly affect the transistor behavior at microwave frequencies [1]-[7], or when new devices are available, as result of an improved technology step process, but an updated foundry model "design kit" has not been developed yet. As consequence, it could be mandatory to extract a custom model, which is more accurate in specific applications. In this context, the choice of the measurements to be used in the extraction of the model parameters is very important and can affect both the extraction time and the accuracy of the model itself. For such a reason, it is essential to have quick and easy identification procedures combined with measurement techniques, which lead to accurate models by means of few measurements and short optimization time.

Unfortunately, reaching a tradeoff between measurement accuracy and simplicity, and identification procedure is a challenging target. Nowadays, a number of efficient transistor model formulations are available [1],[3],[8], but few identification techniques suitable for nonlinear models exist. Alternative approaches disregard theoretical considerations or mathematical representations and rely on huge amount of data to build behavioral models [9]-[12].

Some of the afore mentioned identification techniques are often based on measurements carried out in operating conditions very different from those in which the device actually operates [1], [2],[7]. For example, it is very common to perform dc I/V measurements for the identification of a FET drain current-generator, and multi-bias small-signal ac measurements for the identification of the nonlinear charge sources [8]. As an alternative, I/V pulsed measurements [7], [13]-[16] are commonly used for the identification of a FET drain current-generator and pulsed S-parameter measurements [15]-[16] can be successfully exploited for the identification of nonlinear charge sources. The main advantage of pulsed characterization techniques is that, by studying the influence of the thermal and traps-occupation states on the I/V dynamic characteristics, allows one to gain deep insight in the low-frequency dispersive phenomena affecting microwave transistors [1]-[7]. As well-known, such measurements are far from the actual operation of transistors in nonlinear microwave circuits, such as power amplifiers, mixers, oscillators, switches. Therefore, this imposes stronger requirements on the predictive capability of the model. To overcome these inconveniences, large-signal network analyzer (LSNA) based extraction techniques have been developed [17]-[18], and they have the main advantage of identifying models starting from measurements performed in operating

Manuscript received November 8, 2015. This work was supported by Italian MIUR and FWO – Vlaanderen (Belgium).
V. Vadalà, A. Raffo, and G. Vannini are with the Department of Engineering, University of Ferrara, 44122 Ferrara, Italy (e-mail: antonio.raffo@unife.it).
G. Avolio and D. M. M.-P Schreurs are with the ESAT-Divison TELEMIC, KU Leuven, B-3001 Leuven, Belgium. G. Avolio is a post-doctoral researcher supported by FWO.
M. Marchetti is with Anteverta-mw B.V., Delft, The Netherlands.

conditions which are close to those experienced by the device in actual operations (i.e., sinusoidal or distorted-sinusoidal regime). On the other hand, LSNA-based setups have a frequency limitation more stringent than the frequency bandwidth they can handle (i.e., 67 GHz for today's setups). In fact, when one wants to correctly reconstruct the nonlinear time-domain waveforms of voltages and currents, and use them in the optimization procedure, at least three harmonics have to be acquired. This means that, considering that latest LSNA setups have a maximum bandwidth of 67 GHz, one can set the maximum fundamental frequency up to one-third of such limit. In addition, if one needs to control harmonics, more than three harmonic frequencies have to be acquired, thus further lowering the maximum fundamental frequency.

In this scenario, the dynamic-bias measurement technique [19], [20] and its application to model identification, has been proposed as an alternative to overcome the LSNA frequency limitation while maintaining the actual operating condition of devices in the identification phase. The dynamic-bias measurement technique basically consists in exciting the device under test (DUT) simultaneously with LF large-signal and high-frequency (HF) small-signal excitations. The use of a small signal at HF guarantees that the HF harmonics can be neglected and as consequence the fundamental frequency can be set up to the upper frequency limit of the measurement system. Then, the identification procedure associated with this measurement technique uses the device response at LF to retrieve the drain-source current generator model parameters, and the response at HF to obtain the charge-source model parameters [19],[20]. In [19],[20] dynamic-bias measurements are performed with an LSNA with eight-channel vector-receivers as shown in Fig. 1a.

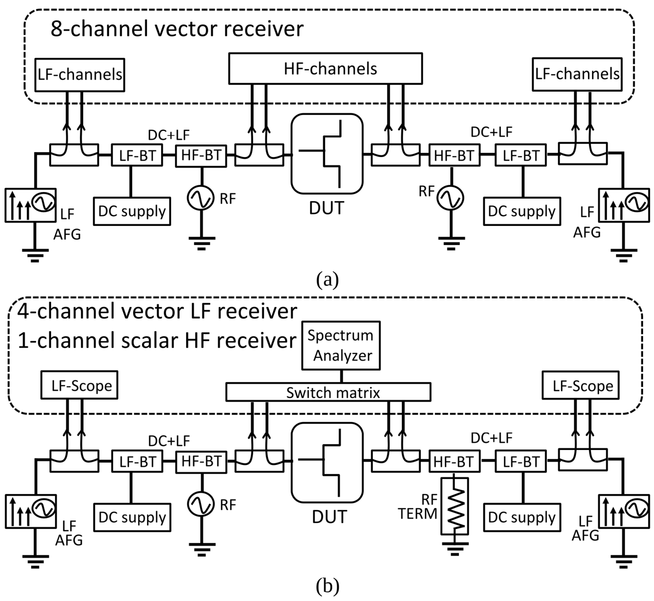

Fig. 1. Dynamic-Bias measurement setup (a) and new proposed architecture with scalar HF acquisition and low-frequency oscilloscope (b).

In this paper, we propose a new setup to perform dynamic-bias measurements. The setup is composed of relatively low-cost instrumentation, commonly available in microwave laboratories. As shown in Fig. 1, the architecture of the proposed setup is different from the one based on an LSNA, like that described in [19]: the "8-channel vector receiver" is replaced by the combination of a "4-channel vector LF receiver" and a "1-channel scalar HF receiver", as shown in Fig. 1b. The choice of the LF receiver is flexible and it can be implemented by means of traditional instrumentation, like an oscilloscope, or by means of acquisition boards. In addition, the simultaneous acquisition of the LF and HF quantities is not required, since in the new architecture a scalar HF receiver is used. The LF excitations are provided by an arbitrary function generator (AFG) with multi-harmonic capability that allows one to set any operating regime at the DUT ports.

The scalar information at HF is successfully used in the optimization phase for the transistor charge model extraction, whereas the vectorial LF information is used for current generator model extraction.

The proposed approach greatly reduces the cost of the whole measurement system, allows a simplified calibration procedure, and at the same time provides measurement data which can be used for model extraction with a good level of accuracy, as will be shown in the following sections.

Despite the proposed measurement technique could appear similar to pulsed S-parameters, it presents significant differences due to the very different operating regime (i.e., traps-occupation and thermal states) that the DUT experiences during the measurement. Consequently, a true comparison between the two approaches is not practically feasible. In addition, the HF quantities gathered by the proposed setup, besides being acquired by imposing actual DUT operating conditions in the identification phase, are scalar whereas in pulsed S-parameters a vector acquisition is performed.

The paper is organized as follow: Section II describes the new approach with some theoretical considerations supported by CAD simulations and explains the proposed measurement setup and calibration procedure. In Section III, the model identification procedure is fully described and in Section IV it is applied to a GaN HEMT device. Finally, Section V reports the model validation by means of HF time-domain harmonic load-pull measurements.

II. Theory and Application of the Proposed Approach

In this section, we describe the new proposed measurement setup and its use to identify a nonlinear model, pointing out the attention on the fact that scalar HF measurements provide enough information to extract an accurate charge-source model.

A. Measurement Technique and Simulations

The dynamic-bias technique [19] consists in exciting the DUT simultaneously with a LF large signal and a HF small signal. As reference for the following, we show in Fig. 2 the frequency spectra of the DUT incident and scattered waves under dynamic-bias operation. The LF large signal allows setting the trap and thermal state of the device [3], [6] (i.e., large-signal operating point, LSOP) whereas the HF small signal, which is named *tickle*, is aimed to stimulate the charge nonlinearities. When the HF tickle is applied on top of the LSOP the charge nonlinearities are gathered in correspondence of this trap and thermal state.

During the dynamic bias measurement, the frequency of the LF signal must be chosen above the cut-off of dispersive phenomena. In this way, the channel temperature and trap occupation state can be considered frozen. Moreover if the frequency of the LF signals is low enough to neglect the nonlinear dynamic phenomena (i.e., nonlinear capacitance), the measured LF I/V characteristics correctly describe the dynamic behavior of the drain-source current generator.

It is important to underline at this point that the excitation at LF can be easily controlled to have a specific load-line (e.g., class AB, class B, class F, etc.) at the current-generator source of the device [21],[22],[23]. This is not achievable when setting the LSOP at microwave frequencies [24] since in such case the load-line can be synthesized only at the extrinsic plane of the device and not at the current generator.

When the DUT is excited with such kind of signals, its response has the harmonic content shown in Fig. 2, which consists of the LF fundamental tone with its harmonics, of the fundamental HF tone and of the intermodulation tones due to the interaction between the LF and HF components [19], [25]. It is important to underline that the HF signal harmonics can be neglected due to the HF small-signal regime [19], [20].

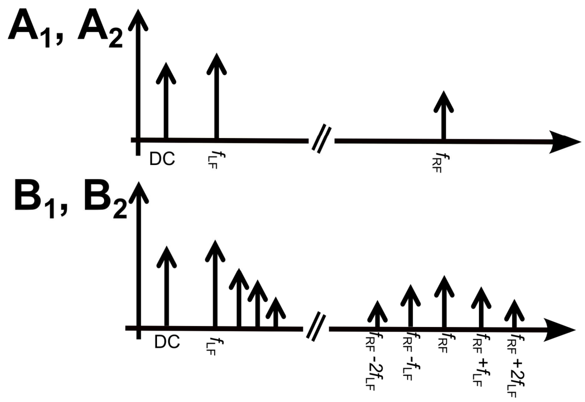

Fig. 2. Spectra of incident and scattered waves under dynamic-bias operation.

Dynamic-bias measurements can be collocated to those class of measurements where a large-signal operating point (i.e., the LF signal) is perturbed by a small-signal (i.e., a HF tickle). From literature [9],[10] it is demonstrated that if the frequency of the tickle is offset with respect to the frequency of the LSOP, the amplitude of intermodulation tones arising from the interaction between the tickle and the LSOP is independent of the tickle phase which can be arbitrary with respect to the phase of the LSOP. This applies also to dynamic-bias measurements and can be intuitively explained by linearizing, for example, the scattered wave B_2 with respect to the LF LSOP. By adopting a formalism similar to the one in [9] we can write:

$$B_2(t) = f[A_1(t), A_2(t)] \tag{1}$$

$$A_1(t) = A_{1,f_{LF}}(t) + \Delta A_{1,f_{RF}}(t) \tag{2}$$

$$A_2(t) = A_{2,f_{LF}}(t) + \Delta A_{2,f_{RF}}(t) \tag{3}$$

$$B_2(t) \approx f[A_{1,f_{LF}}(t), A_{2,f_{LF}}(t)] + \\ + \frac{\partial f}{\partial A_1} \Delta A_{1,f_{RF}}(t) + \frac{\partial f}{\partial A_2} \Delta A_{2,f_{RF}}(t) \tag{4}$$

where $A_1(t), A_2(t), B_1(t), B_2(t)$ are, respectively, the time-varying incident and scattered waves at the input and output ports; $A_{1,f_{LF}}(t), A_{2,f_{LF}}(t)$ are the time-varying incident waves used to set the LSOP, and $\Delta A_{1,f_{RF}}(t), \Delta A_{2,f_{RF}}(t)$ are the HF tickles. We assume that $\Delta A_{2,f_{RF}} = 0$ (i.e., matched load at RF). The time-varying first order derivatives will generate frequency components at nf_{LF} (n = 0, 1, 2,…N). These components are multiplied by the tickles $(\Delta A_{1,f_{RF}}), (\Delta A_{2,f_{RF}})$ producing the intermodulation tones at $f_{RF} \pm nf_{LF}$. It is noteworthy that each intermodulation tone is generated by direct harmonic mixing of the LSOP frequencies and the tickle frequency, and no other intermodulation tone at the same frequency is generated due to higher order mixing. As a consequence, the amplitude of the intermodulation tones is independent, for a fixed LSOP, from the phase of the HF tickle. With the aim to show the validity of this assumption, we performed some simulations under dynamic-bias conditions by using a GaN HEMT device model available in a commercial CAD simulator (i.e., Keysight ADS). The harmonic-balance simulation was performed at the fixed bias V_{d0} = 20 V, I_{d0} = 15 mA, synthesizing at the DUT drain side an impedance Z_{LF} = 100 + j*30 Ω at the fundamental LF (i.e., 2 MHz), and Z_{HF} = 50 Ω at the fundamental HF (i.e., 5 GHz), whereas all the other harmonics were terminated on 50 Ω. At the gate port, a LF large signal with amplitude A_{gLF} = 3 V and a tickle A_{gHF} = 0.2 V were simultaneously applied. Finally, the relative phase of the HF tickle was swept in the range 0°-360° with 5° step. Fig. 3 shows the simulation results. In particular, Fig. 3a and 3b show the time-domain current and voltage waveforms at gate and drain ports for all the swept phase values, drawn with a sufficient number of points to distinguish the HF tickle on top of the LF signal. To make the graph clearer, the time-domain waveforms with only the LF component are highlighted in Fig. 3a and 3b with black dotted tick lines.

Fig. 3c and 3d show, on a polar plot, the phasors of the tickle and of the first two intermodulation tones (i.e., $f_{RF} \pm f_{LF}$, $f_{RF} \pm 2f_{LF}$). In particular, while the phase is changing, the amplitude of the HF tickle and of the intermodulation tones lays on circular trajectories on the polar plot.

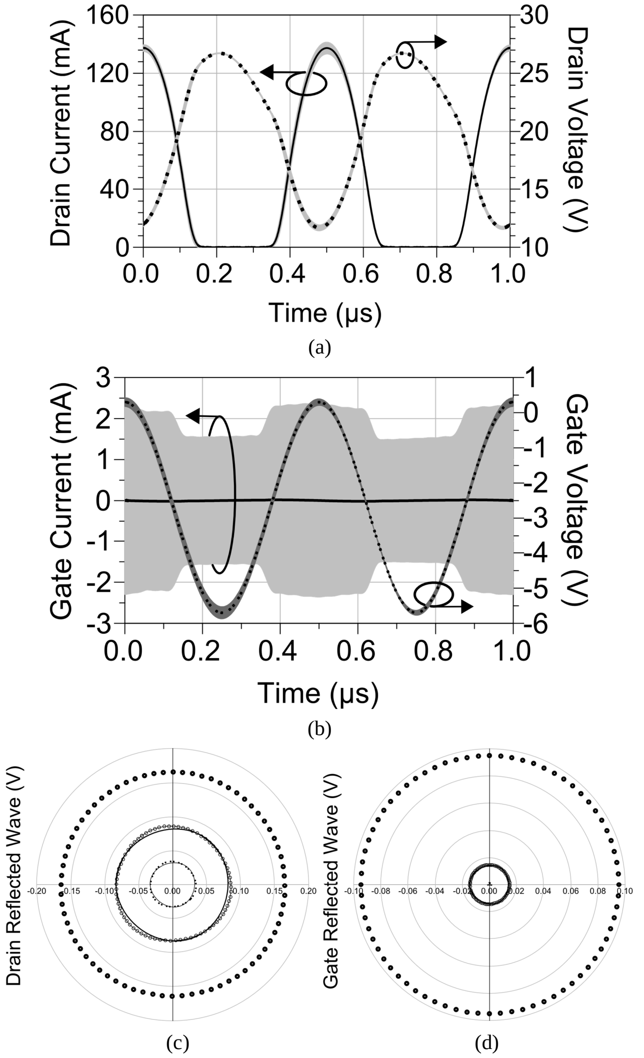

Fig. 3. Time-domain current and voltage at drain (a) and gate (b) device ports. Phasors of the tickle and of the first two intermodulation tones at drain (c) and gate (d) ports.

B. Measurement Setup and Calibration

The new proposed measurement setup, used to carry out dynamic-bias measurements, is shown in Fig. 4. The "4-channel vector LF receiver" is implemented by the PXI5105 Oscilloscope/Digitizer with 60 MSa/s real-time sample rate and 12-bits of resolution. The "1-channel scalar HF receiver" is implemented by a 50-GHz spectrum analyzer (Agilent 8565E).

Two bias tees, with appropriate frequency range, are used to correctly couple dc, LF and HF signals; LF and HF bi-directional couplers are used to separate incident and scattered waves and a two-channel arbitrary function generator and an RF source are used to provide the excitations at LF and HF, respectively. It is important to underline that the LF arbitrary function generator allows the full control of amplitude and phase of the fundamental tone and harmonics so that any operating regime can be easily set directly at the current generator of the DUT [26]. Finally, as we used a one-channel spectrum-analyzer, a switch-matrix was employed to measure the four HF wave magnitude.

The LF and HF paths are separately calibrated. We used a SOLT calibration for the LF path. As regarding the HF path, only scalar information is available and therefore one can account only for the power transfer characteristics of the measurement path.

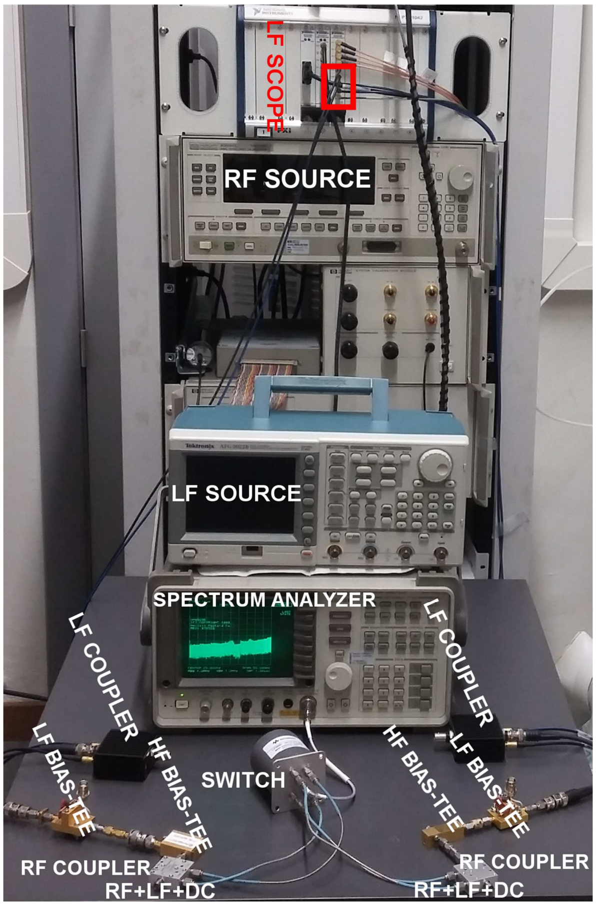

Fig. 4. Proposed Dynamic-bias measurement setup. LF and HF bi-directional couplers and spectrum analyzer, LF oscilloscope and LF and HF sources.

This is typically done, for instance, in case of scalar load-pull setups [27]. As widely known, the complexity reduction gained with a scalar calibration as compared to a vector calibration is paid in terms of accuracy. We show, however, that for the experimental conditions investigated in this work, the scalar calibration provides a measurement accuracy comparable with the one of a vector calibration.

Fig. 5 shows a schematization of the input HF path of the setup in Fig. 1b, represented as a four-port network, and (5) reports the corresponding well-known error model that we assumed in this work. For simplicity, we focus on the input HF path, but the same considerations are clearly valid for the output HF path. In addition, we assume that ports 3 and 4 are perfectly matched, thus a_3 and a_4 in Fig. 5 are equal to zero.

The model can then be reduced to the widely adopted two-port model, or one can measure the S-parameters of the error-boxes with a calibrated network analyzer.

For the scalar calibration, only few terms in the matrix in (5) can be used to derive the magnitude of the waves a_2, b_2 at the DUT reference plane, starting from the magnitude of the raw measured waves b_3 and b_4.

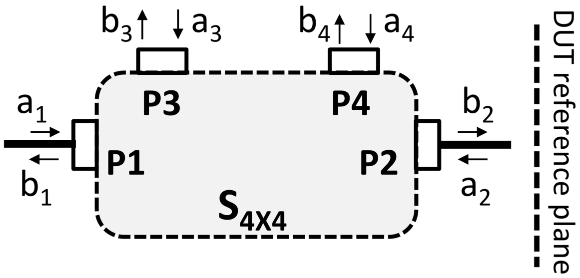

Fig. 5. Four-port error model used in high-frequency calibration.

$$\begin{bmatrix} b_1 \\ b_2 \\ b_3 \\ b_4 \end{bmatrix} = \begin{pmatrix} S_{11} & \cdots & S_{14} \\ \vdots & \ddots & \vdots \\ S_{41} & \cdots & S_{44} \end{pmatrix} \begin{bmatrix} a_1 \\ a_2 \\ a_3 \\ a_4 \end{bmatrix} \quad (5)$$

This four-port error model actually represents the dual-directional coupler and cables used in the HF acquisition paths. The input port of a dual-directional coupler is not coupled with the reverse coupled port so that the corresponding S-parameters (i.e., measured $|S_{32}|$ and $|S_{23}|$) can be considered zero; also the output port is not coupled with the forward coupled port so that the corresponding S-parameters (i.e., measured $|S_{41}|$ and $|S_{14}|$) can be considered zero. The forward and reverse coupled ports are also isolated from each other, therefore S_{34} and S_{43} can be considered negligible. As a consequence, the system reduces to:

$$\begin{bmatrix} b_1 \\ b_2 \\ b_3 \\ b_4 \end{bmatrix} = \begin{pmatrix} S_{11} & S_{12} & S_{13} & 0 \\ S_{21} & S_{22} & 0 & S_{24} \\ S_{31} & 0 & S_{33} & 0 \\ 0 & S_{42} & 0 & S_{44} \end{pmatrix} \begin{bmatrix} a_1 \\ a_2 \\ 0 \\ 0 \end{bmatrix} \Rightarrow$$

$$\Rightarrow \begin{cases} b_1 = S_{11}a_1 + S_{12}a_2 \\ b_2 = S_{21}a_1 + S_{22}a_2 \\ b_3 = S_{31}a_1 \\ b_4 = S_{42}a_2 \end{cases} \Rightarrow \begin{cases} b_1 = S_{11}\, {}^{b_3}\!/_{S_{31}} + S_{12}\, {}^{b_4}\!/_{S_{42}} \\ b_2 = S_{21}\, {}^{b_3}\!/_{S_{31}} + S_{22}\, {}^{b_4}\!/_{S_{42}} \\ a_1 = {}^{b_3}\!/_{S_{31}} \\ a_2 = {}^{b_4}\!/_{S_{42}} \end{cases} \quad (6)$$

The system of equations in (6) cannot be solved starting from scalar measurements unless doing further approximations. For the setup considered in this paper also the return loss of the four ports is quite low and consequently S_{11} and S_{22} can be neglected without introducing important errors. These approximations are valid until the components in the HF calibration path show good performance in the considered frequency range. In particular, by using commercial bidirectional couplers available in our laboratory, we found that the approximation is valid with insertion loss below -15 dB, reverse coupling below -35 dB, and isolation between coupled ports below -60 dB. This allows one to perform the de-embedding of data using only scalar measurements. In this way the modules of a_1 and a_2 can be directly calculated from the modules of the raw measured waves b_3 and b_4, which are the quantities acquired by the spectrum analyzer. Also b_2 and b_1 can be directly calculated from the magnitude of the measured raw waves b_3 and b_4. Therefore, the quantities of interest at the DUT reference plane are:

$$|b_2| = \left|\frac{S_{21}}{S_{31}}\right| \cdot |b_3| \quad (7)$$

$$|a_2| = \left|\frac{b_4}{S_{42}}\right| \quad (8)$$

The above assumptions greatly simplify the calibration procedure and their validity and accuracy is demonstrated by the good agreement with vector-corrected (i.e., considering all the terms in (5)) measurements carried out by means of a LSNA (see Fig. 7 and Table II). In order to fairly compare the results, we used an LSNA (see Fig. 1a) to perform dynamic-bias measurements and we corrected the acquired raw waves (i.e., b_3 and b_4) by applying both a vector and scalar calibration to obtain the waves at the DUT reference plane, a_2 and b_2. We performed dynamic-bias measurements on a 0.25-µm GaN HEMT biased at V_{d0} = 20 V and I_{d0} = 15 mA. The frequency of the HF tickle is f_{RF} = 5 GHz, whereas the LSOPs are set at f_{LF} = 2 MHz for three different conditions, namely 3.5+j*11.6 Ω, 50 Ω, and 106 - j*57 Ω. The HF load was constant and close to 50 Ω. In Fig. 6 we show the LF dynamic output characteristics for the three different dynamic-bias measurements. For the LSOP corresponding to 50 Ω we report in Fig. 7 the spectrum magnitudes of the input and output scattered waves after applying vector (circles) and scalar (crosses) calibrations. In Table I we also report the comparison between the two calibration procedures for the magnitude of the incident input HF tickle.

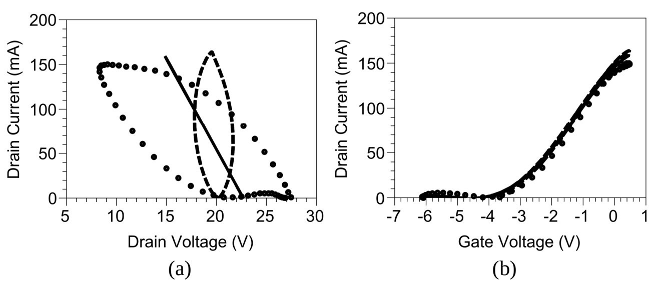

Fig. 6. Measured dynamic characteristics for three LSOPs: short (dashed line), 50 Ω (solid line), and 106 - j*57 Ω (circles).

Finally, Table II reports the comparison between the two calibration procedures for the spectrum magnitudes of the input and output reflected waves for the LSOPs corresponding to the 3.5+j*11.6 -Ω and 106 - j*57 -Ω load. From these comparisons, we can deduce that, despite the additional approximations, the scalar calibration yields very similar results compared to the vector one.

TABLE I
COMPARISON BETWEEN SCALAR AND VECTORIAL CORRECTED MAGNITUDE OF INCIDENT WAVES FOR THE 50-Ω LOAD

Frequency	a_1 (dBm)	
	scalar	vectorial
f_{RF}	-24.90	-24.742

III. IDENTIFICATION PROCEDURE

Measurements performed by means of the new measurement setup are used to implement an extraction procedure for nonlinear transistor modelling. The spectrum resulting from dynamic-bias measurements is composed of LF and HF components as shown in Fig. 2. When we excite the DUT with LF signals, de facto, we are fixing the trap and thermal states of the DUT without exciting the charges (i.e., the capacitances behave as an open at a few megahertz).

On the other hand, it is worth noticing that the HF small signal does not modify the trap and thermal states which are settled by the LF excitation. This situation is similar to multi-bias S-parameter measurements as the slowly-varying LF large signal behaves as a "constant voltage" with respect to the HF tickle.

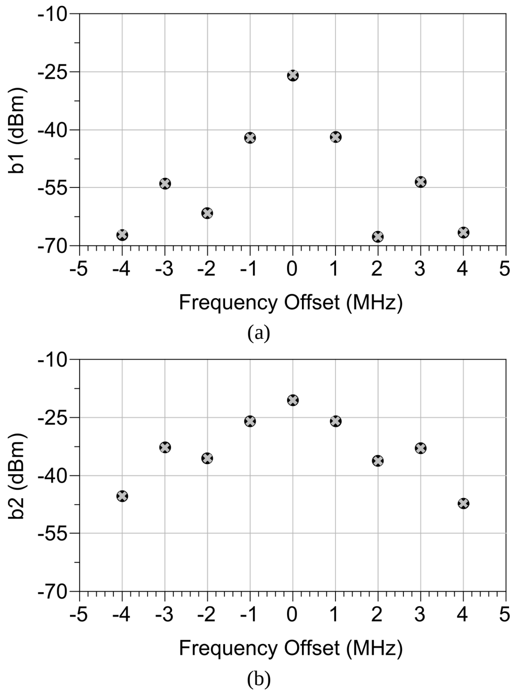

Fig. 7. Measured (a) input and (b) output HF spectra of scattered waves after vector (crosses) and scalar (circles) calibration.

The voltage values assumed along the whole LF waveform are the equivalent of the dc values in conventional multi-bias S-parameters, but with the additional advantage that the bias variation is obtained with one single LF load-line. By imposing suitable load-lines, information on conduction currents and charge states can be gathered from the pinch-off to the saturation regions and in all the intermediate conditions, and used for the accurate extraction of the model.

The extraction procedure is based on the assumption that LF components are strictly related to the current-generator source and the HF components are strictly related to the charge sources [3],[6],[21]. In particular, we use only the LF spectrum to extract the parameters of the drain current-generator source. Once these parameters are extracted, we use the HF spectrum to identify the charge-source parameters.

The flowchart in Fig. 8 summarizes the steps of the identification procedure.

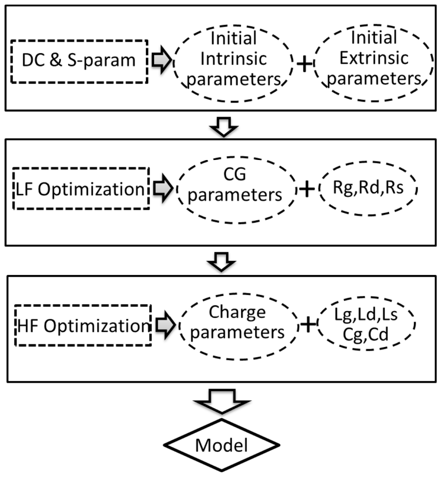

Fig. 8. Flowchart of the model identification procedure by using the dynamic bias-measurement technique [19], [20].

The first step consists in identifying the initial parameters to set in the optimization. This step is carried out by using few dc and S-parameter measurements [28]. Then, by means of the LF spectrum data, the current generator parameters and resistive parasitic elements (i.e., R_g, R_d, R_s) are extracted. In this optimization step the error function is defined by considering only the LF components according to (9). Once this numerical optimization reaches the goal and the optimal current-generator parameters are found, the current-generator model is kept constant and the HF spectrum scalar data are used for the extraction of the charge-source parameters and reactive parasitic elements. In this optimization step the error function is defined by considering only the HF tickle and the intermodulation tones according to (10). At the end of this step the nonlinear model is available. The error functions in the LF optimizations are defined by means of the real and imaginary parts of scattered waves as in (9):

$$
\begin{aligned}
\mathrm{E}_{LF}(k) = \sum_k \Big(& \left|\mathrm{Re}\left\{bs_{1,2}(k) - bm_{1,2}(k)\right\}\right| + \\
& + \left|\mathrm{Im}\left\{bs_{1,2}(k) - bm_{1,2}(k)\right\}\right| \Big)^2 , \\
& k = nf_{LF},\ n = 0,1,..,5.
\end{aligned}
\tag{9}
$$

HF error functions are defined by means of the magnitude of scattered waves as in (10):

$$
\begin{aligned}
\mathrm{E}_{HF}(k) = \sum_k & \left(\left|bs_{1,2}(k)\right| - \left|bm_{1,2}(k)\right| \right)^2 , \\
& \left\{ k = f_{HF} \pm nf_{LF} \quad n = 0,1,2,3,4. \right.
\end{aligned}
\tag{10}
$$

TABLE II
COMPARISON BETWEEN SCALAR AND VECTORIAL CORRECTED MAGNITUDE OF REFLECTED WAVES FOR TWO DIFFERENT LOADS

Frequency	3.5 + j*11.6 Ω				106 – j*57 Ω			
	b_1 (dBm)		b_2 (dBm)		b_1 (dBm)		b_2 (dBm)	
	scalar	vectorial	scalar	vectorial	scalar	vectorial	scalar	vectorial
f_{RF} - $4f_{LF}$	-67.216	-67.066	-45.293	-45.284	-73.067	-73.012	-47.816	-47.813
f_{RF} - $3f_{LF}$	-53.976	-53.979	-32.776	-32.776	-54.045	-54.03	-31.535	-31.533
f_{RF} - $2f_{LF}$	-61.614	-61.619	-35.53	-35.53	-67.329	-67.318	-33.874	-33.875
f_{RF} - f_{LF}	-42.056	-42.063	-26	-26.004	-40.272	-40.277	-26.31	-26.314
f_{RF}	-26.068	-25.802	-20.535	-20.542	-26.229	-25.949	-20.992	-20.999
f_{RF} + f_{LF}	-41.912	-41.92	-25.892	-25.901	-40.727	-40.733	-26.993	-27.001
f_{RF} + $2f_{LF}$	-67.704	-67.677	-36.204	-36.216	-58.283	-58.274	-34.048	-34.059
f_{RF} + $3f_{LF}$	-53.507	-53.526	-32.966	-32.978	-53.13	-53.144	-31.989	-32
f_{RF} + $4f_{LF}$	-66.598	-66.565	-47.208	-47.228	-63.999	-64.029	-47.026	-47.031

In (9) and (10), k is the harmonic component, $bm_{1,2}(k)$ are the measured scattered waves at the gate and drain, respectively, and $bs_{1,2}(k)$ are the simulated ones.

In the next section, we apply the procedure to extract the model of a 0.25-µm GaN HEMT device with the aim of validating the effectiveness, for accurate model extraction, of the characterization technique performed by the new measurement setup.

IV. MODEL EXTRACTION

The proposed measurement setup, jointly with the identification procedure, was used for the identification of a 0.25-µm x 200-µm GaN HEMT nonlinear model. In this work we adopted the Angelov model [8], even if any analytic formulation that describes the current generator and charges can be used as well. The model was extracted at the fixed bias V_{d0} = 20 V and I_{d0} = 15 mA. For the LF excitation signal, the fundamental frequency f_{0LF} = 2 MHz was considered adequate to be above the cutoff of the dispersive phenomena [26], whereas the frequency of the tickle was set equal to f_{0HF} = 5 GHz.

Dynamic-bias measurements were carried out by means of the proposed measurement setup on the selected device, synthesizing 7 different loading conditions corresponding to class-AB and class-F operation at the current-generator plane and performing, for each load, an input power sweep (i.e., sweep of incident LF wave at the gate port). For each of these conditions, an HF tickle of -20 dBm of power was superimposed on top of the LF excitation at the input HF port of the device, whereas the output HF port was terminated on 50 Ω. Fig. 9 and Fig. 10 show some measurements carried out on the DUT and used for model identification. In particular, Fig. 9 shows the spectra of the incident and scattered waves, whereas Fig. 10 shows the load-lines corresponding to different impedances synthesized in class-AB and class-F operation (i.e., for different LSOPs) and for different input power levels. Following the identification procedure described in Section III, we used the LF spectra of these measurements to set the numerical optimization devoted to the extraction of the current-generator source and resistive parasitic element models. Fig. 9 and Fig. 10 show the fitting capability of the model after the first numerical optimization step.

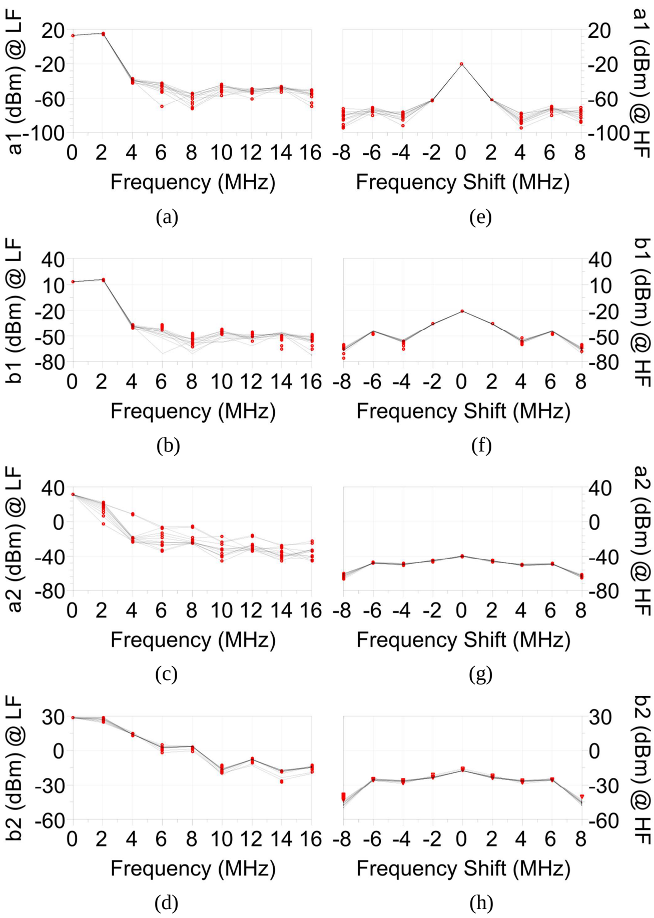

Fig. 9. Measured (symbols) and simulated (lines) spectra at LF and HF. The horizontal axis in the HF spectrum represents the shift from f_{0HF}. Bias: V_{D0} = 20 V, I_{D0} = 15 mA, f_{0LF} = 2 MHz, f_{0HF} = 5 GHz.

Once we found the optimal current-generator model parameters, the second optimization step was performed where the HF measured spectra in Fig. 9 were used to set the numerical optimization devoted to the extraction of the charge-source parameters. Looking at Fig. 9 you can see also the fitting capability of the model after this second optimization step. Considering the error definition in (10), the

This is the author's version of an article that has been published in this journal. Changes were made to this version by the publisher prior to publication.
The final version of record is available at https://doi.org/10.1109/TMTT.2016.2628748

accuracy of the charge-source model has to be evaluated looking at the HF components of the scattered waves. The model parameters obtained after the extraction procedure are reported in Table III.

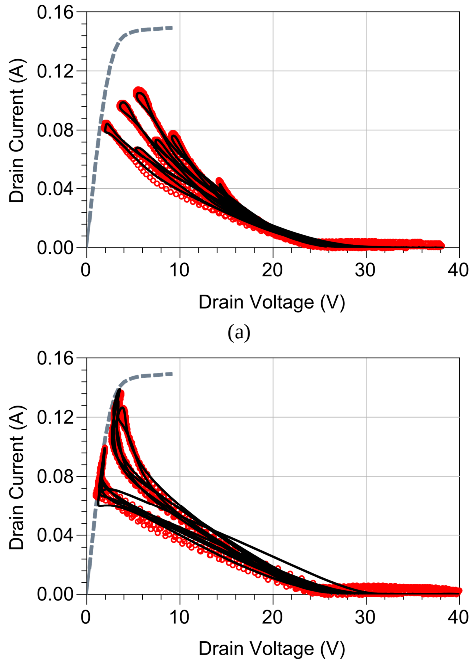

(b)

Fig. 10. Measured (circles) and simulated (lines) load-lines for class AB (a) and class F (b) operation as a function of the input power level: V_{D0} = 20 V, I_{D0} = 15 mA, f_{0LF} = 2 MHz. Measured dc output characteristic at V_{G0} = 0 V is also shown (dashed line).

V. Model Validation

The extracted model was validated by means of active harmonic load-pull measurements carried out at f_0 = 5 GHz [29] at the DUT quiescent bias condition V_{D0} = 20 V, I_{D0} = 15 mA. A relatively low HF frequency (i.e., 5 GHz) was chosen in order to make the harmonic load-pull validation feasible and acquiring at least five harmonics. The harmonic load-pull characterization carried out for the validation consists in four steps:

1) Load-pull @ f_0.
2) Load-pull @ $2f_0$, keeping constant Z@ f_0.
3) Load-pull @ $3f_0$, keeping constant Z@ f_0 and $2f_0$.
4) Load-pull @ f_0, $2f_0$ and $3f_0$.

In the first step, load-pull measurements at the fundamental frequency were performed in order to find the optimal impedances both for output power and drain efficiency. Fig. 11 shows the comparison between measured and simulated output power and efficiency contours at 3.5 dB of gain compression. In Table IV we report the comparison between measured and simulated output power and drain efficiency values for the optimal impedances in Fig. 11.

In Fig. 12 the comparison between measured and simulated load-lines, input loci and the transistor performance (i.e., output power and gain) over the entire P_{av} sweep is shown for the optimal impedances in Fig. 11.

In the second step, second harmonic load-pull measurements were carried out by keeping constant the fundamental impedance at $Z_{tradeoff}$=122 +j*127 Ω, obtained from step 1 as the best tradeoff between output power and efficiency.

TABLE III
Model Parameters

Extrinsic parasitic elements					
Rg (Ω)	1.6	*Rd* (Ω)	3.9	*Rs* (Ω)	0.0
Lg (pH)	161	*Ld* (pH)	152	*Ls* (pH)	1.6
Cg (fF)	26.6	*Cd* (fF)	37.6		
Current Generator Model Parameters					
Ipk0	0.084	*Vpks*	-1.1	*Δvpks*	0.8
P1	0.52	*P2*	-0.035	*P3*	0.027
αr	$8.5e^{-7}$	*αs*	0.22	*λ*	0.003
B1	1.25	*B2*	0.56	*Rth*	30.2
Cth	0.0001	*Tcipk0*	-0.00032	*Tcp1*	-0.004
Charge Model Parameters					
Cds(fF)	115	*Cgspi*(fF)	240	*Cgs0*(fF)	37
Cgdpi(fF)	46	*Cgd0*(fF)	32		
P10	6.5	*P11*	2.7	*P20*	-0.1
P21	0.25	*P30*	-0.22	*P31*	0.02
P40	4.5	*P41*	0.33		

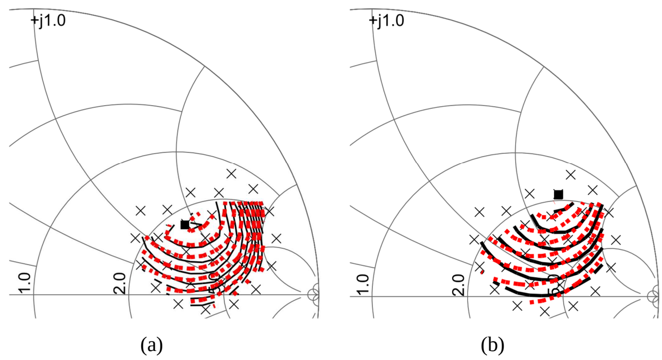

(a) (b)

Fig. 11. Measured (black solid line) and simulated (red dashed lines) output power (a) and drain efficiency (b) contours at 3.5-dB gain compression. In (a) the inner circle is at 27 dBm with step 0.5 dB. In (b) the inner circle is at 54 % with step 5%. Filled square is the optimum impedance. f_0 = 5 GHz.

TABLE IV
Measured and Simulated Pout and Efficiency at Optimal Impedances

	Pout (dBm)	Zpout (Ω)	Efficiency (%)	Zeff (Ω)
Measured	27.08	*117+j*87*	54	91.9+j*143.3
Simulated	27.01	*117+j*86*	54	92.3+j*142.8

In the third step, third harmonic load-pull measurements were carried out by keeping constant the fundamental impedance at $Z_{tradeoff}$=122 +j*127 Ω and the second harmonic impedance at Z_{2ndopt}=1.5 +j*50 Ω, which represent the optimal condition for efficiency. Finally, in the fourth step we performed harmonic load-pull measurements by sweeping few impedances around the optimal conditions at the first, second, and third harmonics, in order to refine the search.

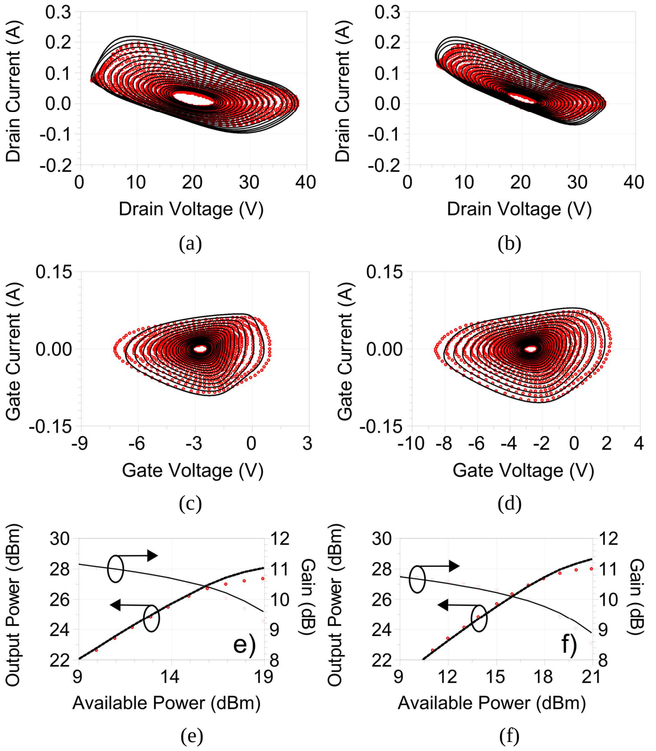

Fig. 12. Measured (symbols) and simulated (lines) load-lines ((a) and (b)), input loci ((c) and (d)), output power and gain ((e) and (f)) for the two loads corresponding to the optimum for output power (a),(c),(e) and efficiency (b),(d),(f) at 5 GHz.

Fig. 13 shows the measured impedance grids and the results of the comparison between measurements and simulations for the second, third and fourth step of the harmonic load-pull characterization, which are named respectively case 1, case 2 and case 3. In particular, the output power and drain efficiency are shown, for the three cases considered, at constant input power for all the synthesized impedances. Fig. 13 also shows the load lines and input loci for the optimal second and third harmonic impedances. The gate current and voltage are excellent indicators of the accuracy of the charge-source model whereas the output power, power added efficiency, and drain current and voltage are more strictly related to the current-generator source model accuracy. The good agreement between measured and simulated input loci shown in Fig. 13 confirms the accuracy of the nonlinear charge-source model as well as the well fitted drain quantities validate the accuracy of the current-generator model under very different operating conditions. In the fourth and last measurement step, which is case 3 in Fig. 13, we performed load-pull measurements at fundamental, second and third harmonics. We report the comparison between measurements and simulations for this case. The accuracy of the extracted model is again confirmed by the good agreement between measured and simulated gate and drain characteristics. The good prediction obtained in the several synthesized conditions represents a definitive validation of the effectiveness of using scalar HF data for the extraction of the charge-source model.

VI. Conclusion

In this work, for the first time, dynamic-bias measurements carried out by using scalar acquisition of HF data were used to extract a nonlinear transistor model. The proposed method greatly simplifies the measurement setup and the calibration procedure of the HF part of the setup even though guarantees good level of accuracy for the extracted models. In addition, the system becomes cheaper and easily implementable by means of instrumentations typically present in microwave laboratories.

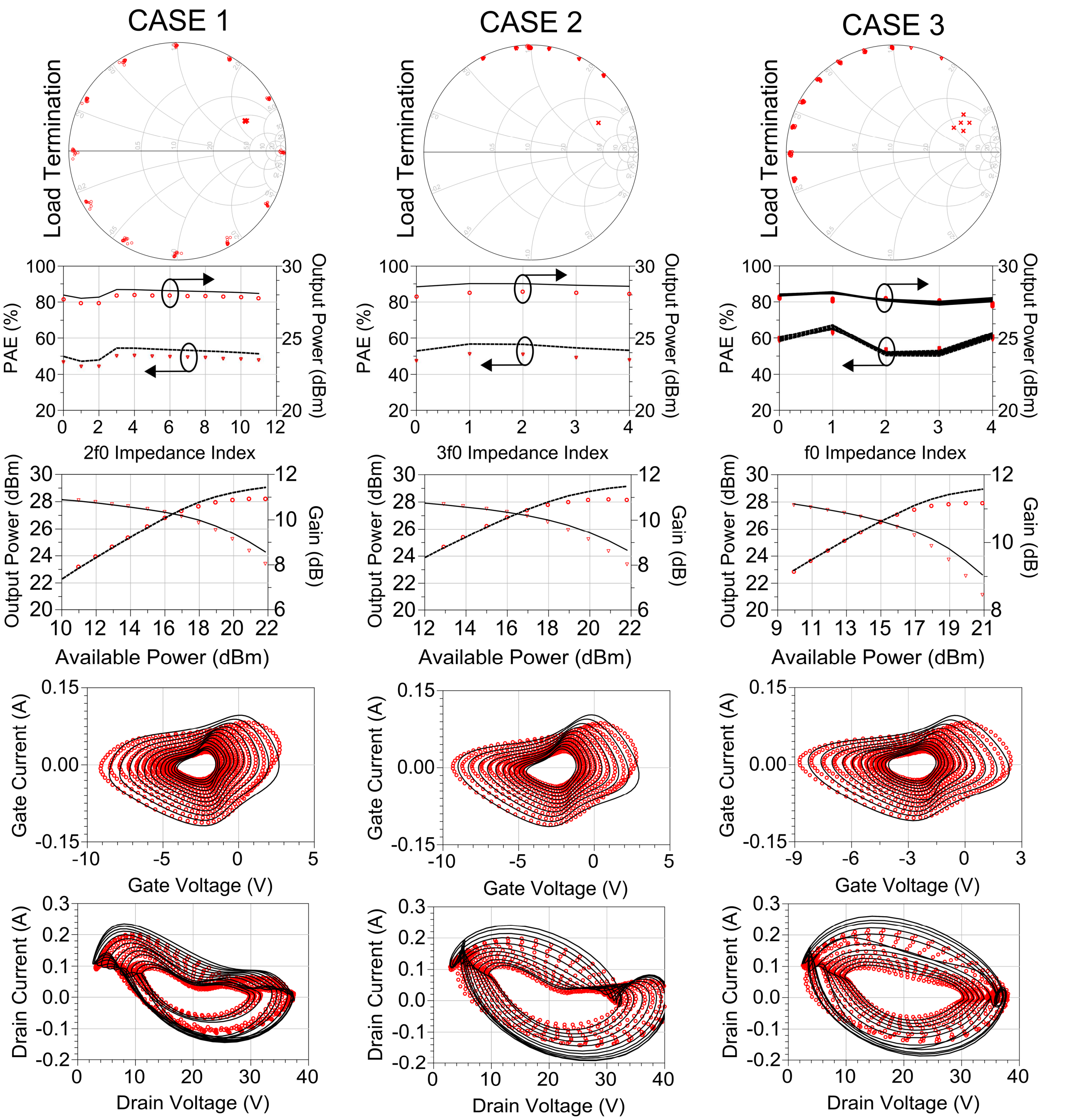

Fig. 13. Load pull at second harmonic (case 1). Load pull at third harmonic (case 2). Load pull at first, second and third harmonic (case 3). From top to bottom in each column: measured impedance grids; PAE and output power at fixed P_{av} of 19 dBm (case 1), 20 dBm (case 2), and 18 dBm (case 3); output power and gain, load lines, and input loci as a function of available input power for the loads corresponding to the optimal efficiency. Measures (symbols) and simulations (lines). f_0 = 5 GHz.

References

[1] L. Dunleavy, C. Baylis, W. Curtice, and R. Connick, "Modeling GaN: powerful but challenging," *IEEE Microw. Mag*., vol. 11, no. 6, pp. 83–96, Oct. 2010.

[2] J. Rodriguez-Tellez, T. Fernandez, A. Mediavilla, and A. Tazon, "Characterization of thermal and frequency-dispersion effects in GaAs MESFET devices," *IEEE Trans. Microw. Theory and Techn.*, vol.49, no. 7, pp. 1352–1355, Jul. 2001.

[3] A. Raffo, V. Vadalà, D. M. M.-P. Schreurs, G. Crupi, G. Avolio, A. Caddemi, and G. Vannini, "Nonlinear dispersive modeling of electron devices oriented to GaN power amplifier design," *IEEE Trans. Microw. Theory and Techn.*, vol. 58, no. 4, pp. 710-718, Apr. 2010.

[4] G. Meneghesso, G. Verzellesi, R. Pierobon, F. Rampazzo, A. Chini, U. K. Mishra, C. Canali, and E. Zanoni, "Surface-related drain current dispersion effects in AlGaN-GaN HEMTs," *IEEE Trans. Electron Devices*, vol. 51, no. 10, pp. 1554–1561, Oct. 2004.

[5] J. Joh and J. A. del Alamo, "A current-transient methodology for trap analysis for GaN high electron mobility transistors," *IEEE Trans. Electron Devices*, vol. 58, no. 1, pp. 132–140, Jan. 2011.

[6] A. Raffo, G. Bosi, V. Vadalà, and G. Vannini, "Behavioral modeling of GaN FETs: a load-line approach," *IEEE Trans. Microw. Theory and Techn.*, vol. 62, no. 1, pp. 73–82, Jan. 2014.

[7] A. Santarelli, D. Niessen, R. Cignani, G.P. Gibiino, P.A. Traverso, C. Florian, D.M.M.-P. Schreurs, and F. Filicori, "GaN FET nonlinear modeling based on double pulse I/V characteristics," *IEEE Trans. Microw. Theory and Techn.*, vol.62, no.12, pp.3262-3273, Dec. 2014.

[8] I. Angelov, N. Rorsman, J. Stenarson, M. Garcia, and H. Zirath, "An empirical table-based FET model," *IEEE Trans. Microw. Theory and Techn.*, vol. 47, no. 12, pp. 2350-2357, Dec. 1999.

[9] D.E Root, J. Verspecht, D. Sharrit, J. Wood, A. Cognata, "Broad-band poly-harmonic distortion (PHD) behavioral models from fast automated simulations and large-signal vectorial network measurements," *IEEE Trans. Microw. Theory and Techn.*, vol.53, no.11, pp.3656-3664, Nov. 2005.

[10] J. Verspecht, and D. E. Root, "Poly harmonic distortion modeling". *IEEE Microw. Magazine*, vol. 7, no. 3, pp. 44-57, Jun. 2006.

[11] H. Qi, J. Benedikt, and P. J. Tasker, "Nonlinear data utilization: from direct data lookup to behavioral modeling," *IEEE Trans. Microw. Theory and Techn.*, vol. 57, no. 6, pp.1425-1432, Jun. 2009.

[12] J. Cai, J. King, B. Merrick, and T. Brazil, "Padé-approximation-based behavioral modeling," *IEEE Trans. Microw. Theory and Techn.*, vol. 61. no. 12, pp. 4418-4427, Dec. 2013.

[13] J.P. Teyssier, P. Bouysse, Z. Ouarch, D. Barataud, T. Peyretaillade, and R. Quere, "40 GHz/150-ns versatile pulsed measurement system for microwave transistor isothermal characterization," *IEEE Trans. Microw. Theory and Techn.*, vol. 46, no. 12, pp. 2043-2052, Dec. 1998.

[14] F. Filicori, G. Vannini, A. Santarelli, A. M. Sanchez, A. Tazon, and Y. Newport, "Empirical modeling of low-frequency dispersive effects due to traps and thermal phenomena in III-V FET's," *IEEE Trans. Microw. Theory and Techn.*, vol. 43, no. 12, pp. 2972-2981, Dec. 1995.

[15] T. Fernandez, Y. Newport, J. M. Zamanillo, A. Tazon, and A. Mediavilla, "Extracting a bias-dependent large signal MESFET model from pulsed I/V measurements," *IEEE Trans. Microw. Theory and Techn.*, vol. 44, no. 3, pp. 372-378, Mar. 1996.

[16] J. Scott, J. G. Rathmell, A. Parker, and M. Sayed, "Pulsed device measurements and applications," *IEEE Trans. Microw. Theory and Techn.*, vol. 44, no. 12, pp. 2718-2723, Dec. 1996.

[17] D. Schreurs, J. Verspecht, B. Nauwelaers, A. Van de Capelle, and M. Van Rossum, "Direct extraction of the non-linear model for two-port devices from vectorial non-linear network analyzer measurements," *Eur. Microw. Conf.*, pp. 921-926, Sep. 1997.

[18] M.C. Curras-Francos, P. J. Tasker, M. Fernandez-Barciela, S.S. O'Keefe, Y. Campos-Roca, and E. Sanchez, "Direct extraction of nonlinear FET I-V functions from time domain large signal measurements," *Electron. Lett.*, vol. 34, no. 21, pp. 1993-1994, Oct. 1998.

[19] G. Avolio, A. Raffo, I. Angelov, V. Vadalà, G. Crupi, A. Caddemi, G. Vannini, and D. M. M.-P. Schreurs, "Millimeter-Wave FET nonlinear modelling based on the dynamic-bias measurement technique," *IEEE Trans. Microw. Theory and Techn.*, vol. 62, no. 11, pp. 2526-2537, Nov. 2014.

[20] V. Vadalà, A. Raffo, G. Avolio, M. Marchetti, D.M.M.-P. Schreurs, and G. Vannini, "Extraction of accurate GaN HEMT model for high-efficiency power amplifier design," *IEEE MTT-S Int. Microw. Symp. Dig.*, pp. 1-4, 17-22, May 2015.

[21] A. Raffo, F. Scappaviva, and G. Vannini, "A new approach to microwave power amplifier design based on the experimental characterization of the intrinsic electron-device load line," *IEEE Trans. Microw. Theory and Techn.*, vol. 57, no. 7, pp. 1743–1752, Jul. 2009.

[22] A. Raffo, P. Colantonio, E. Cipriani, V. Vadalà, G. Bosi, T. M. Martin-Guerrero, G. Vannini, and F. Giannini, "Theoretical consideration on harmonic manipulated amplifiers based on experimental data," *in Proc. IEEE International Workshop on Integrated Nonlinear Microwave and Millimetre-wave Circuits (INMMiC)*, pp. 1-3, Oct. 2015.

[23] A. Musio, V. Vadalà, F. Scappaviva, A. Raffo, S. Di Falco and G. Vannini, "A new approach to Class-E power amplifier design," *in Proc. IEEE International Workshop on Integrated Nonlinear Microwave and Millimetre-wave Circuits (INMMiC)*, pp. 1-4, Apr. 2011.

[24] J. Verspecht, "Large signal network analysis", *IEEE Microw. Mag.*, vol. 6, no. 4, pp. 82-92, Dec. 2005.

[25] G. Paillончy, G. Avolio, M. Myslinski, Y. Rolain, M. Vanden Bossche, and D. Schreurs, "Large-signal network analysis including baseband," *IEEE Microw. Mag.*, vol. 12, no. 2, pp. 77-86, Mar. 2011.

[26] A. Raffo, S. di Falco, V. Vadalà, and G. Vannini, "Characterization of GaN HEMT low-frequency dispersion through a multiharmonic measurement system," *IEEE Trans. Microw. Theory and Techn.*, vol. 58, no. 9, pp. 2490-2496, Sep. 2010.

[27] A. Ferrero, U. Pisani, "An improved calibration technique for on-wafer large-signal transistor characterization," *IEEE Trans. Instrumentation and Measurement*, vol. 42, no. 2, pp. 360-364, Apr 1993.

[28] G. Crupi and D. M. M.-P. Schreurs, *Microwave de-embedding: from theory to application*. Oxford, UK: Academic Press, 2013.

[29] M. Marchetti, M.J. Pelk, K. Buisman, W. Neo, M. Spirito, and L.C.N.de Vreede, "Active harmonic load–pull with realistic wideband communications signals," *IEEE Trans. Microw. Theory and Techn.*, vol. 56, no. 12, pp. 2979-2988, Dec. 2008.

Valeria Vadalà (S'07 - M'11) was born in Reggio Calabria, Italy, in 1982. She received the M.S. degree (Hons.) in electronic engineering from the Mediterranea University of Reggio Calabria, Reggio Calabria, in 2006, and the Ph.D. degree in information engineering from the University of Ferrara, Ferrara, Italy, in 2010.

She is currently with the Department of Engineering, University of Ferrara, as a Post-Doctoral Researcher. Her current research interests include nonlinear electron-device characterization and the modeling and circuit-design techniques for nonlinear microwave and millimeter-wave applications.

Antonio Raffo (S'04–M'07) was born in Taranto, Italy, in 1976. He received the M.S. degree (Hons.) in electronic engineering and the Ph.D. degree in information engineering from the University of Ferrara, Ferrara, Italy, in 2002 and 2006, respectively.

Since 2002, he has been with the Engineering Department, University of Ferrara, where he is currently a Research Associate and teaches courses in semiconductor devices and electronic instrumentation and measurement. His current research interests include nonlinear electron device characterization and the modeling and circuit-design techniques for nonlinear microwave and millimeter-wave applications. He has co-authored over 100 publications in international journals and conferences and co-edited *Microwave Wireless Communications: From Transistor to System Level* (Oxford, U.K.: Elsevier, 2016).

Dr. Raffo is a member of the Technical Programme Committee of the IEEE International Workshop on Integrated Nonlinear Microwave and Millimetrewave Circuits (INMMiC) and the IEEE Microwave Measurement Technical Committee (MTT-11). He serves as an Associate Editor for the *International Journal of Numerical Modelling: Electronic Networks, Devices and Fields*, and was the Technical Programme Committee Chair of the IEEE INMMiC Conference, Leuven, Belgium, 2014.

Gustavo Avolio (M' 12) was born in Cosenza, Italy, in 1982. He received the MSc. in electronic engineering from the University of Calabria, Italy, in 2006.

In 2012 he obtained the Ph.D. in electronic engineering from KU Leuven, Belgium. He is currently a post-doctoral researcher supported by FWO Vlaanderen, Belgium. In 2013 and 2014 he has been a visiting scientist at the National Institute of Standards and Technology (NIST) in Boulder, USA. Since 2009 he has been a visiting scientist at the University of Ferrara, Italy.

His research work focuses on large-signal measurements and nonlinear modeling of advanced microwave devices.

Mauro Marchetti Mauro Marchetti received the B.S. degree (cum laude) and the M.Sc. degree (cum laude) in electrical engineering from the University of Naples "Federico II," Naples, Italy, in 2004 and 2006 respectively, and the Ph.D. degree from Delft University of Technology, Delft, The Netherlands, in 2013.

In 2006 he joined the Electronics Research Laboratory, Delft University of Technology where he carried out his Ph.D. research on the development of advanced characterization setups for RF high-power and high-linearity amplifier design.

In 2010 he co-founded and was appointed CEO of Anteverta-mw B.V., a company providing pioneering solutions in the fields of device characterization and high performance power amplifier design.

His research interests include the development of advanced characterization setups for RF high-power and high-linearity amplifier design.

Giorgio Vannini (S'87 – M'92) received the Laurea degree in electronic engineering and Ph.D. degree in electronic and computer science engineering, from the University of Bologna, Bologna, Italy, in 1987 and 1992, respectively.

He joined the Department of Electronics of the University of Bologna as a Research Associate in 1992. Since 1994 to 1998 he has also been with CSITE, Bologna (Research Centre on Electronics, Computer science and Telecommunication Engineering, National Research Council), where he has been responsible of the MMIC testing and CAD laboratory.

In 1998 he joined the University of Ferrara as an Associate Professor and since 2005 as a Full Professor of Electronics. He was Head of the Engineering Department from 2007 to 2015, and member of the Board of Directors from 2010 to 2012.

During his academic career he has been a Teacher of applied electronics, electronics for communications and industrial electronics. He has co-authored over 250 papers devoted to electron device modelling, computer-aided design techniques for MMICs, and nonlinear circuit analysis and design.

Giorgio Vannini is a cofounder of the academic spinoff Microwave Electronics for Communications (MEC) and a member of the Technical Scientific Committee of the "MIST E-R" Laboratory for Industrial Research and Technology Transfer.

Dominique M. M.-P. Schreurs (S'90–M'97–SM'02-Fellow) received the M.Sc. degree in electronic engineering and Ph.D. degree from the Katholieke Universiteit Leuven, Leuven, Belgium.

She is currently a Full Professor with the Katholieke Universiteit Leuven. She has been a Visiting Scientist with Agilent Technologies, Santa Rosa, CA, USA, ETH Zürich, Zürich, Switzerland, and the National Institute of Standards and Technology, Boulder, CO, USA. Her main research interests concern the (non)linear characterization and modeling of active microwave devices, and (non)linear circuit design for telecommunications and biomedical applications.

Dr. Schreurs serves on the AdCom of the MTT Society and also serves as an Editor-in-Chief for the IEEE TRANSACTIONS ON MICROWAVE THEORY AND TECHNIQUES and as the Vice-President on the Executive Committee of the ARFTG organization. She was the General Chair of the 2007 and 2012 Spring ARFTG Conference and the Co-Chair of the European Microwave Conference in 2008. She was an MTT-S Distinguished Microwave Lecturer.

.